4 FEL Physics

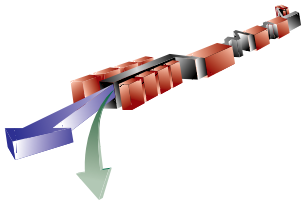

TECHNICAL SYNOPSIS

This chapter presents a review of the historical and technological developments of the Free Electron Laser that led to proposals to operate an FEL in the large gain regime, starting from the spontaneous radiation noise, without using an optical cavity. In this mode, called "Self-Amplified-Spontaneous-Emission" (SASE), lasing is produced in a single pass of an electron beam with high phase-space density through a long undulator, eliminating the need for optical cavities, which are difficult to build in the soft x-ray or x-ray spectral region.

A discussion of the spontaneous radiation produced in an undulator introduces the concepts and formulae for the radiation intensity, the number of photons produced per electron, brightness, and peak power. The spontaneous radiation is emitted incoherently, and its intensity increases linearly with the number of electrons. In an FEL, the intensity grows with the square of the number of electrons and the number of photons produced per electron is increased by many orders of magnitude. This is achieved by using the FEL collective instability, which produces microbunching of the electrons on the scale of the optical wavelength of the radiation. The microbunching and the radiation intensity grow exponentially. The inverse of the growth rate is called the FEL gain length.

Several conditions must be satisfied for the collective FEL instability to occur. A parameter of paramount importance is the electron density in phase space. The scaling laws for a SASE-FEL, derived using these conditions, and the desire to minimize the undulator length define how the beam's 6-dimensional phase space density must increase as the radiation wavelength is decreased.

The time structure of the radiation pulse is determined by the electrons' slippage with respect to the radiation that they produce and by the fact that the FEL starts from the noise or fluctuations in the initial particle longitudinal distribution. The slippage in one gain length determines the cooperation length. The output radiation pulse comes in the form of spikes of random phase and amplitude and with a width of the order of the cooperation length.

In addition to the fundamental wavelength, the SASE process results in harmonics with significant intensity. The intensity of the third harmonic is about 1% of the intensity of the fundamental and extends the radiation wavelength range of the FEL to 0.5 Å.

These theoretical predications have been confirmed in a series of experiments. Large amplification of the spontaneous undulator radiation, reaching the saturation level, has been

demonstrated in SASE FEL experiments in the infrared, visible, and UV spectral regions. Saturation has been observed at wavelengths as short as 98 nm. The experimental results on the gain length, saturation and the intensity fluctuation distribution are in good agreement with the FEL collective instability theory.

The pulse length and linewidth of the x-ray pulses from the LCLS can be controlled and improved over the LCLS initial design, by manipulating the electron beam and/or the radiation pulse and with the use of multiple undulators. The possibility offered by the LCLS to study and develop these methods is important, and depends critically on the electron beam quality and the choice of undulator length and gap.

4.1 Introduction

Undulator radiation, particularly useful because of its small line width and high brightness, is being used in many synchrotron radiation sources built around the world and provides at present the brightest source of x-rays. For long undulators, the free-electron laser (FEL) collective instability gives the possibility of much larger x-ray intensity and brightness. The instability produces an exponential growth of the radiation intensity, together with a modulation of the electron density on the scale of the radiation wavelength. The radiation field initiating the instability is the spontaneous radiation field, or a combination of the spontaneous radiation field and an external field. In the first case the FEL is called a Self-Amplified Spontaneous Emission (SASE) FEL. If the external field is dominant it is called an FEL amplifier.

The FEL is a system consisting of a relativistic electron beam and a radiation field, interacting with each other while they propagate through an undulator. The undulator magnetic field generates an electron velocity component transverse to the direction of propagation. The transverse velocity couples the electron beam to the electric field component of the radiation field, thus producing an energy exchange between them. The coupling can lead to the formation of density modulations (structures), collective modes, in the electron beam, and to the generation of coherent electromagnetic radiation. The formation of structures also enhances the energy exchange. As a result, the transition from the original unstructured state of the electron beam to the collective state is an exponential process. This chapter discusses the physics of this process; some of the experimental results obtained recently, and the development of x-ray FELs.

The FEL is the result of many years of theoretical and experimental work on the generation of radiation from relativistic electron beams. The first generators of coherent electromagnetic (EM) radiation from electron beams were the microwave tubes. Their development received a strong impulse during World War II. Microwave tubes use slow wave structures, a fact that limits their operation mainly to long wavelengths, i.e., in the centimeter region. FELs were developed from the work on free electron beams. Motz [1] showed in 1951 that an electron beam propagating through an undulator magnet could be used to amplify radiation. The Ubitron, a microwave tube developed in 1960 by Philips [2], is quite similar to the FEL. Theoretical work on FELs was done in the 1960s and 1970s by Palmer [3], Robinson [4] and Csonka [5].

During the 1960s, the research on the generation of short wavelength coherent radiation turned mainly in the direction of atomic and molecular lasers, and optical resonators. While extremely successful in the infrared (IR), visible and UV, these lasers have limited tunability, and this line of development has limitations at shorter wavelengths. While soft x-ray lasers have been built at several laboratories, such as the University of Colorado, Princeton, and Livermore, their extension to the Ångstrom region is problematic. The use of electron beams and FELs is an alternative when atomic and molecular lasers and microwave tubes cannot be used. Madey [6], in 1971, analyzed again the possibility of exchanging energy between free electrons and electromagnetic radiation in the small gain regime, using a quantum theoretical approach. He and his coworkers followed this work with successful experimental demonstration of a FEL amplifier [7], and an FEL oscillator [8] at 10 μm. This very important step led over the following years to a large interest in free-electron lasers, and to the successful construction and operation of many FEL oscillators, at wavelengths from the far IR to the near UV. These FEL oscillators operated in the small-signal gain regime, using the optical cavity as a feedback device starting from the spontaneous synchrotron radiation noise.

While the existence of an exponentially growing solution for the FEL equations has been studied by many authors [9], the first theory of a SASE FEL in the 1-dimensional (1-D) case, including the start from spontaneous radiation and saturation, was given in [10]. This theory describes all of the FEL physics, including saturation power and undulator saturation length, with one single quantity, the FEL parameter, ρ, a function of the electron beam density and energy, and of the undulator period and magnetic field. Further studies clarified the initiation process and its connection with spontaneous radiation [11]. The next important step was the extension of the theory to three dimensions (3-D) [12] to include diffraction effects and to show the existence of optical guiding. More recent work has extended the 3-D model to include also the initiation process [13] and the betatron motion [14].

The first proposal to use the FEL collective instability to produce infrared radiation using a single pass amplifier starting from noise was published by Kondratenko and Saldin in 1980 [15]. The first proposal to use the instability using a single pass amplifier starting from noise for a soft x-ray FEL was published by Murphy and Pellegrini in 1985 [16]. The choice of a single pass amplifier instead of an oscillator in the soft or hard x-ray region is motivated by the fact that optical cavities have large losses and that they are difficult to build and operate at these wavelengths.

An analysis of the scaling laws [17] for a single pass FEL, starting from noise, shows that the gain of a SASE-FEL depends on wavelength, and that to reach the soft or hard x-ray region one needs an electron beam with a large six dimensional phase-space density, a condition, which until recently, was difficult to satisfy.

The Murphy–Pellegrini proposal used a bypass in a storage ring to provide the electron beam. At that time, an electron storage ring was the accelerator delivering an electron beam with the highest phase space density. However, the limitations on emittance, peak current, and energy

spread due to the storage ring collective effects, such as the microwave instability or the Touschek effect, limited the shortest FEL wavelength to about a few hundred Ångstroms.

The development of radio frequency photocathode electron guns [18], and the emittance compensation method [19] has changed this situation. At the same time the work on linear colliders has demonstrated that it is possible to accelerate and time compress electron beams without spoiling their brightness [20]. At a Workshop on Fourth Generation Light Sources held at SSRL in 1992 it was shown [21] that using these new developments one could build a 0.1 to 1 nm SASE FEL. This work led to further studies [22] and to two major proposals, LCLS at SLAC [23] and TESLA at DESY [24] for a 0.1 nm SASE-FEL, with peak power of the order of tens of GW, pulse length of about 230 fs (FWHM) or shorter, full transverse coherence, and peak brightness about ten orders of magnitude larger than that of third generation synchrotron radiation sources.

While the theory of the SASE FEL has been developed starting in the 1980s, experimental results have been obtained only during the last few years, initially in the infrared to visible region of the spectrum, and more recently at wavelengths as short as 80 nm [25, 26, 27, 28, 29, 30, 31, 32, 33, 34, 35, 36], the shortest wavelength reached by an FEL to date. The data agree well with the theoretical predictions on exponential growth and its dependence on electron beam parameters and on the intensity fluctuations. These results give us confidence that the present theory can be used to design an x-ray SASE FEL.

This chapter starts with a general overview of FEL physics in **Section 4.2** and continues, in **Section 4.3**, with a review of the recent results of SASE experiments in the infrared, visible and ultra-violet wavelength-regime. **Section 4.4** introduces the specific situation of the LCLS. The effects of the emission of ordinary undulator radiation on the FEL process is analyzed in **Section 4.5**. The effects of undulator vacuum chamber wakefields on the performance of the LCLS are assessed in **Section 4.6**. **Section 4.7** discusses an option of emittance and charge control based and **Section 4.8** evaluates options for x-ray pulse length and linewidth reduction that will be available as an upgrade of the present LCLS design.

4.2 Free-electron Laser Physics

4.2.1 Coherent Undulator Radiation from a Single Electron

The emission of radiation from relativistic electrons traveling through an undulator is reviewed. The reader is referred to other books or papers, as for instance reference [37], for a more general discussion. For a planar or helical undulator the radiation is emitted at the wavelength

$$\lambda_r = \frac{\lambda_u}{2\gamma^2}(1 + a_u^{\,2} + \gamma^2\theta^2) \qquad \textbf{(4.1)}$$

where λ_u is the undulator period, γmc^2 the beam energy, $a_u = e\langle B_u^2\rangle^{1/2} c\lambda_u / 2\pi mc^2$ is the undulator parameter, B_u is the undulator transverse magnetic field, $\langle B_u^2\rangle^{1/2}$ is the rms over one undulator period, and θ is the angle between the undulator axis and the direction at which the radiation is observed. Note, the relation between the frequently used undulator parameter, K, and a_u is $K = a_u$

(for a helical undulator) and $K= a_u\sqrt{2}$ (for a planar undulator.) For reasons described in **Chapter 8**, a planar undulator was chosen for the LCLS. The rms width of the radiation line (bandwidth) on axis, θ=0, is related to the number of undulator periods N_u by

$$\frac{\Delta\omega}{\omega} = \frac{1}{N_u}. \tag{4.2}$$

The undulator is an extended linear source, but the coherent part of the radiation within the on-axis bandwidth **Eq. (4.2)** can be approximately described as an equivalent source at the undulator center, with rms divergence

$$\sigma'_c = \sqrt{\frac{\lambda_r}{\lambda_u N_u}}, \tag{4.3}$$

and an effective rms source radius (diffraction limited)

$$\sigma_c = \frac{1}{4\pi}\sqrt{\lambda_r \lambda_u N_u}. \tag{4.4}$$

Notice that the product

$$\sigma_c \sigma'_c = \frac{\lambda_r}{4\pi}, \tag{4.5}$$

is the minimum phase space area for a diffraction-limited photon beam.

The intensity of the radiation emitted on axis, at the wavelength given by **Eq. (4.1)** and its harmonics n, per unit frequency and solid angle is

$$\frac{d^2 I}{d\omega d\Omega} = \frac{N_u^2 e^2 \gamma^2}{c} \frac{a_u^2}{1+a_u^2} F_n(a_u), \tag{4.6}$$

where

$$F_n(a_u) = \{J_{(n-1)/2}(\zeta) - J_{(n+1)/2}(\zeta)\}^2 n^2,$$
$$\zeta = \frac{a_u^2}{2(1+a_u^2)}, \tag{4.7}$$

for a planar undulator. (n=1 is the fundamental). For a helical undulator $F_1(a_u)$=1 for the fundamental and $F_n(a_u)$=0 for harmonics, i.e., n>1.

The coherent intensity is obtained by multiplying **Eq. (4.6)** by the solid angle corresponding to **Eq. (4.3)**, $\Delta\Omega_c=\pi\sigma'^2_c$ and the bandwidth given by **Eq. (4.2)**. Dividing this intensity by the photon energy allows to rewrite the coherent intensity as the number of photons per electron, within the same solid angle and line width, as

$$N_{ph} = \frac{\pi\alpha}{2} \frac{a_u^2}{\left(1+a_u^2\right)} F_1(a_u), \tag{4.8}$$

where α is the fine structure constant. For a typical value a_u~1, one obtains N_{ph}~10^{-2}, showing that the undulator radiation process is rather inefficient.

4.2.2 Coherent Spontaneous Radiation from Many Electrons

To avoid an increase in the radiation linewidth, angular spread, and transverse radius, the relative rms energy spread, σ_E / E, radius, σ, and angular divergence, σ', of the electron beam must be matched to the radiation linewidth $1/N_u$, radius, σ_c, and angular divergence, σ_c'. N_u is the number of undulator periods. This gives the conditions

$$\frac{\sigma_E}{E} \le \frac{1}{N_u} \tag{4.9}$$

$$\sigma \le \sigma_c \tag{4.10}$$

$$\sigma' \le \sigma_c' . \tag{4.11}$$

The last two conditions can be written, using Eq. (4.5), as

$$\varepsilon = \sigma\sigma' \le \frac{\lambda}{4\pi}, \tag{4.12}$$

where ε is the transverse beam emittance. The last condition can be seen as "phase space matching" of the electrons and photons.

The radiation generated from different electrons entering the undulator at different points in time $t_{o,k}$ (where k is an index of the electrons) along the bunch differs only by a phase factor. The electric field at frequency $\omega = 2\pi c/\lambda_r$ can be written as

$$E_k = E_0 e^{i\omega t_{o,k}} , \tag{4.13}$$

where E_0 is a common factor. The total electric field is then proportional to the bunching factor,

$$B_0 = \frac{1}{N_e}\sum_{k=1}^{N_e} e^{i\omega t_{0,k}} , \tag{4.14}$$

where N_e is the number of electrons in the bunch. For a short undulator, i.e., short with respect to the FEL gain length defined in the next section, the bunching parameter does not appreciably change as the beam propagates through the undulator, but, as can be seen below, it can change in the case of a long undulator. In the "short undulator" case the total intensity is then

$$I = I_0 \,|\, B_0 \,|^2 \; N_e{}^2 . \tag{4.15}$$

Three cases can be considered:

a. Uniform beam current: This corresponds to a uniform distribution the electron phases with respect to radiation wave, giving B_0=0 and I=0;

b. Bunch length much shorter than the radiation wavelength: Then $|B_0|^2$~1. In this case the radiation from all electrons has the same phase and the intensity is proportional to the square of the number of electrons and can be called coherent radiation;

c. In most cases, as for instance when the electron beam is generated by a thermionic cathode or by a photocathode, and when the bunch length is longer than the wavelength, the quantity B_0 is a random number, changing for each

electron bunch that is produced. Averaging over many bunches one has $<B_0>=0$, and $<|B_0|^2>\sim 1/N_e$.

This discussion assumes a classical picture of the electron beam and of the electromagnetic radiation. Quantum effects will be discussed later and are small in the LCLS case.

Considering now the emission of radiation by many electrons within the coherent solid angle and the line width defined before, in case c, when there is no correlation between the field emitted by each one of them, the total number of photons emitted is simply

$$N_{ph} = \frac{\pi\alpha}{2} N_e \frac{a_u^{\,2}}{1+a_u^{\,2}} F_1(a_u). \qquad \textbf{(4.16)}$$

If case b would apply this number would be larger by another factor N_e, a very large enhancement.

4.2.3 SASE-FELs

In this section only the main results are considered and the reader is referred to the many papers already given as references for a more complete discussion.

The physical process on which an FEL is based is the emission of radiation from one relativistic electron propagating through an undulator. However collective effects can lead to interesting new situations when many electrons interact with the undulator and the radiation fields. Consider the emission of coherent radiation from N_e electrons, that is the radiation at the wavelength λ_r, **Eq.**(4.1), within the coherent solid angle $\pi\sigma_c^2$, **Eq. (4.3)**, and line width $\Delta\omega/\omega$, **Eq. (4.2)**.

When there is no correlation between the fields generated by each electron, as in the case of spontaneous radiation, the total number of coherent photons emitted, given by **Eq. (4.16)**, is about 1% of the number of electrons. If all electrons were within a radiation wavelength the number of photons would increase by a factor N_e. Even when this is not the case, and the electron distribution on the scale of λ_r is initially random, the number of photons per electron is increased by the FEL collective instability, which produces an exponential growth of the intensity and of the bunching parameter

$$B_z = \frac{1}{N_e}\sum_{k=1}^{N_e} e^{i\omega t_{z,k}}\ , \qquad \textbf{(4.17)}$$

where $t_{z,k} = z_k / v_k$ is the time for electron k, moving with the longitudinal velocity v_k, to reach the longitudinal position z_k. The growth saturates when the bunching parameter becomes of the order of one. For a long undulator the coherent intensity grows along the undulator as

$$I \sim \frac{I_0}{9}\exp(z/L_G), \qquad \textbf{(4.18)}$$

where L_G is the exponential growth rate, called the power gain length, and I_0 is the spontaneous coherent undulator radiation intensity for an undulator with a length L_G, and is proportional to the square of the initial value of the bunching factor, $|B_0|^2$.

The instability growth rate, or gain length, is given in a 1-D model by [10]

$$L_G = \frac{\lambda_u}{4\sqrt{3}\pi\rho}, \tag{4.19}$$

where ρ is the FEL parameter

$$\rho = \left(\frac{a_u}{4\gamma} \sqrt{F_1(a_u)} \frac{\Omega_p}{\omega_u} \right)^{2/3}, \tag{4.20}$$

$\omega_u = 2\pi c/\lambda_u$ is the undulator frequency, $\Omega_p = (4\pi c^2 r_e n_e/\gamma)^{1/2}$ is the beam plasma frequency, n_e is the electron density, and r_e is the classical electron radius. A similar exponential growth occurs if there is an initial input field that dominates any noise in the beam, i.e. amplified stimulated emission.

In the SASE case, saturation occurs after about 20 power gain lengths, and the radiated energy at saturation is about $E_{sat} = \rho N_e E$ [10], where E is the total kinetic energy of the electron beam. The number of photons per electron at saturation is then $N_{sat} = \rho E/E_{ph}$, where E_{ph} is the energy of a single photon. For an x-ray FEL with $E_{ph} \sim 10^4$ eV, $E \sim 15$ GeV, $\rho \sim 0.5\times10^{-3}$ one obtains $N_{sat} \sim 10^3$, i.e., an increase of almost 5 orders of magnitude in the number of photons per electron.

The instability can develop only if the undulator length is much larger than the power gain length, and some other conditions are satisfied:

a. Beam emittance of the order of or smaller than the wavelength:

$$\varepsilon \le \frac{\lambda}{4\pi} \tag{4.21}$$

b. Beam relative energy spread smaller than the FEL parameter:

$$\sigma_E / E < \rho \tag{4.22}$$

c. Power gain length shorter than the radiation Rayleigh range:

$$L_G < L_R \tag{4.23}$$

where the Rayleigh range is defined as $L_R = 2\pi\sigma_0^2/\lambda_r$, and σ_0 is the radiation rms beam radius.

Condition a. says that the electron beam must match the transverse phase-space of the radiation. Condition b. limits the electron beam energy spread, and condition c. requires that more radiation be produced than is lost by diffraction. Conditions a. and c. depend on beam radius and radiation wavelength, and are not independent from each other. If they are satisfied, the 1-D model can be used with good approximation. If they are not satisfied the gain length is larger than the 1-D value, **Eq. (4.19)**, as in the LCLS reference case where the emittance $\varepsilon \sim 3\times(\lambda/4\pi)$. In these cases, it is convenient to introduce an effective FEL parameter, which includes three dimensional effects, defined as

$$\rho_{eff} = \frac{\lambda_u}{4\sqrt{3}\pi L_{G3D}}, \tag{4.24}$$

where L_{G3D} is the three dimensional gain length obtained from numerical simulations that includes diffraction and emittance effects.

4.2.4 Slippage, Fluctuations and Time Structure

When propagating in vacuum, the radiation field is faster than the electron beam, and it moves forward, "slips", by one wavelength, λ_r, per undulator period. The slippage distance in one gain length defines the "cooperation length" [38]

$$L_c = \frac{\lambda_r}{\lambda_u} L_G . \tag{4.25}$$

For a SASE FEL, the undulator radiation field at the frequency $\omega = 2\pi\lambda / c$, is proportional to $\boldsymbol{B}(\omega)$, the Fourier component of the initial bunching factor B_0 at ω. The beam is generated either from a thermionic cathode or from a photocathode. The initial bunching and its Fourier component $\boldsymbol{B}(\omega)$, are random quantities. The initial value of B_0 is different for each beam section of length λ_r, and has a random distribution. The average values are then

$$\left\langle \boldsymbol{B}(\omega) \right\rangle \sim \left\langle \boldsymbol{B}_0 \right\rangle = 0 \tag{4.26}$$

and

$$\left\langle \left| \boldsymbol{B}(\omega) \right|^2 \right\rangle \sim \left\langle \left| \boldsymbol{B}_0 \right|^2 \right\rangle = \frac{1}{N_e} . \tag{4.27}$$

As the electron beam and the radiation propagate through the undulator, the FEL interaction introduces a correlation on the scale length of $2\pi L_c$, producing spikes in the radiation pulse and a random intensity distribution. The number of spikes is [38, 39] $M=L_B/(2\pi L_c)$, where L_B is the rms bunch length. The total energy probability distribution in the x-ray pulse is a Gamma distribution function

$$P(W) = M^M \frac{W^{M-1}}{< W >^M \Gamma(M)} \exp(-MW / < W >) , \tag{4.28}$$

where $<W>$ is the average energy of the x-ray pulse. The standard deviation of this distribution is $1/M^{1/2}$. The line width is approximately the same as for the spontaneous radiation, $\Delta\omega/\omega \sim 1/N_u$.

4.2.5 Nonlinear Harmonic Generation

In a high-gain FEL strong bunching at the fundamental wavelength can drive substantial bunching and, for a planar undulator, significant emitted power at the harmonic frequencies [40]. This nonlinear harmonic generation occurs naturally in one long undulator for a SASE FEL with an initially uniform bunch, as well as in the second stage of a high-gain harmonic generation (HGHG) FEL [41] using a density-modulated bunch. Thus, such a harmonic generation mechanism may be utilized to reach shorter radiation wavelengths or to relax some stringent requirements on the electron beam quality for x-ray FELs.

A three-dimensional theory of harmonic generation in a high-gain FEL has been developed [42] using the coupled Maxwell-Klimontovich equations that include electron energy spread and

emittance, radiation diffraction and guiding, and nonlinear harmonic interactions. In general, each harmonic field is a sum of a linear amplification term and a term driven by nonlinear harmonic interactions. After a certain stage of exponential growth, the dominant nonlinear term is determined by interactions of the lower nonlinear harmonics and the fundamental radiation.

As a result, parameters such as gain length, transverse profile, and temporal structure of the first few harmonics are eventually governed by those of the fundamental. For example, for SASE FELs, driven by the third power of the radiation field in the fundamental, the third nonlinear harmonic grows three times faster, is transversely coherent (with a smaller spot size), and has a more spiky temporal structure than the fundamental wavelength.

Using the LCLS parameters, the transverse profiles of the third nonlinear harmonic and the fundamental radiation are calculated in the exponential growth regime [42]. The third nonlinear harmonic (at 0.5 Å) is also transversely coherent but has a smaller spot size than the fundamental because of the nonlinear generation mechanism. From this analysis one obtains for the third harmonic power [42]

$$\frac{P_3}{\rho P_{beam}} \approx 0.11 \times \left(\frac{P_1}{\rho P_{beam}} \right)^3 , \qquad \textbf{(4.29)}$$

where P_{beam} is the total electron beam power, and P_1 is the fundamental radiation power.

The nonlinear harmonic radiation discussed here is generated when the fundamental frequency component of the FEL radiation bunches the electron beam strongly, producing Fourier components at higher harmonics. Thus, as long as the laser fundamental saturates after a certain length of undulator, the nonlinear harmonics are generated at certain levels, and are less sensitive to electron-beam parameters, undulator errors and wakefield effects than is true for other (linear) harmonic generation schemes. The most significant nonlinear harmonic generation occurs at the third harmonic, whose power approaches one percent of the fundamental power level near saturation. The even harmonics are also present due to the transverse gradient of the beam current. They normally have much lower power levels than their odd counterparts [42]. As discussed in another section, wakefields can reduce the power in the fundamental and one can expect a reduction also in the higher harmonics.

4.2.6 Quantum Effects in Free-Electron Lasers

The quantum theory of free-electron lasers has been studied by several authors, and a review of this work can be found in [43, 44]. More recently, a many-electron quantum theory for a high gain SASE-FEL, like the LCLS, has been developed to look again at possible effects on the FEL start-up, and on the gain length [45].

Quantum effects in the FEL become important when the electron beam wave function exhibits degeneracy and the electrons can no longer be treated as distinguishable particles. The wave function will not be degenerate if the number of electrons in the beam is much less than the number of available states. This will be the case when the beam is sufficiently dilute such that the wave functions of the individual electrons do not overlap, i.e., $\varepsilon_\perp^2 \varepsilon_L >> N_e \lambda_c^3$, where $\varepsilon_\perp$ and ε_L

are the transverse and longitudinal emittance respectively, N_e is the number of electrons, and λ_c is the Compton wavelength. This condition is well satisfied for LCLS parameters.

Quantum corrections to the classical theory become important when the electron beam becomes sensitive to the recoil due to the emission or absorption of discrete photons. The recoil will be small provided the photon energy is much less than the energy emitted per electron at saturation $\hbar\omega << \rho E_{\text{beam}}$, where ω is the radiation frequency and E_{beam} is the electron beam energy. The electron recoil due to discrete photon emission will result in an increased energy spread and therefore an increase in power gain length. The one-dimensional power gain length increases as $L_G / L_{\text{class}} \cong 1 + (\hbar\omega / \rho E_{\text{beam}})^2 / 36$, for $(\hbar\omega / \rho E_{\text{beam}}) < 1$, where L_{class} is the power gain length predicted by classical theory. For the LCLS case $\rho E_{\text{beam}} / \hbar\omega \cong 816$, and the corrections are negligible.

Quantum fluctuations in the position and momentum of the electron beam will also act as effective bunching (i.e., noise) in the electron beam resulting in enhanced start-up of the SASE process. The effective bunching due to the quantum fluctuations will be of the order of $(\hbar\omega / \rho E_{\text{beam}})$ compared to the classical shot noise and therefore will be small for LCLS parameters.

4.3 Experimental Results on SASE-FELs

Until the mid 1990s, very large gain in the SASE mode had been observed only at millimeter wavelengths [25]. After that the experimental studies of SASE FEL physics intensified. The first gain in the infrared wavelength regime at values between 2 to 10 has been observed at Orsay [26] and UCLA [27] and gain in the visible spectral region at Brookhaven [28]. Larger gain in the infrared has also been observed at Los Alamos [29], and gain as large as 3×10^5 at 12 μm has been measured by a UCLA-LANL-RRCKI-SSRL collaboration [30].

The intensity distribution function has been measured for spontaneous undulator radiation, with no amplification and long bunches [46] and, more recently, for amplified radiation and a short bunch length [27, 30].

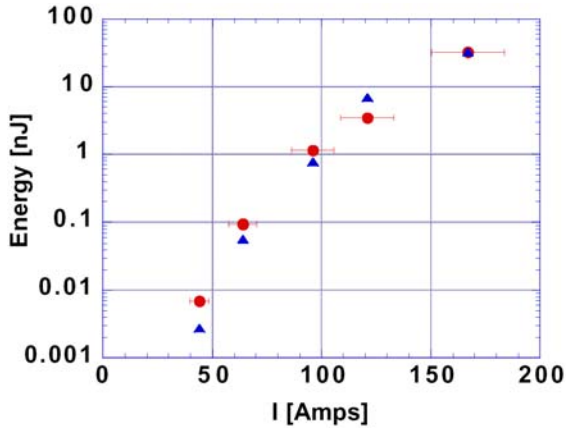

Figure 4.1 Measured values of the mean FEL intensity (circles) versus beam current, compared with a Ginger simulation (triangles) for the UCLA-LANL-RRCKI-SSRL 12 μm SASE-FEL [30].

Results from the UCLA-LANL-RRCKI-SSRL experiment are shown in **Figure 4.1** and **Figure 4.2**. An increase in output intensity by about 10^4 occurs when changing the electron charge by a factor of seven and the peak current by a factor of four as shown in **Figure 4.1**. The change of bunch radius, energy spread, and length with charge makes it difficult to have a simple analytical model to evaluate the gain. The experimental data and the theory have been compared using the simulation code GINGER [47], and the measured values of electron parameters. The results, plotted in **Figure 4.1**, agree with the data within experimental errors. At 2.2 nC the measured gain was 3×10^5, the largest measured, until recently, in the infrared. The intensity fluctuations, shown in **Figure 4.2**, are well described by a Gamma distribution function (**Eq. (4.28)**) with the *M* parameter evaluated from the experimental data in agreement with the theory. The results have also been analyzed independently in reference [48], and again have been found to be in agreement with the theory.

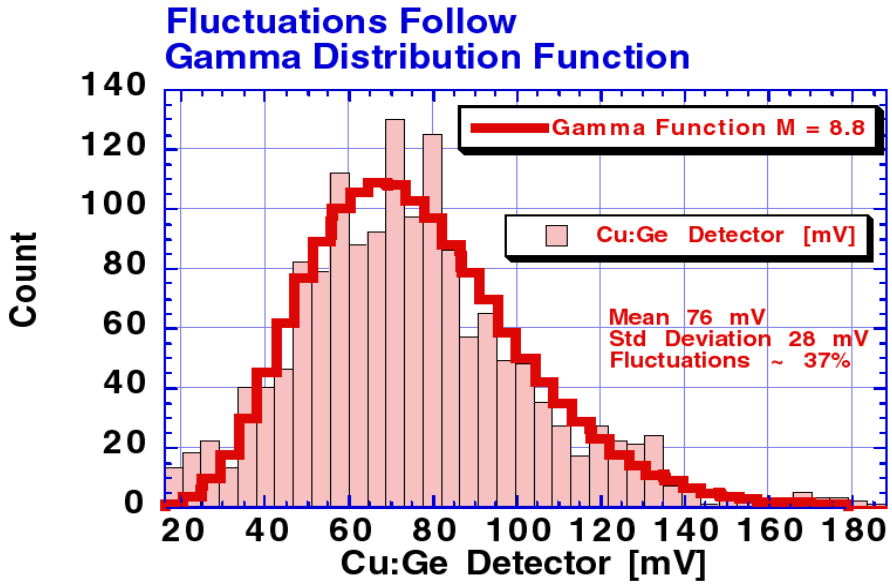

Figure 4.2 Intensity distribution over many events for the same experiment. The experimental data are fitted with a Gamma function distribution [30].

More recently, a BNL group [31] has demonstrated high gain harmonic generation, seeding the FEL with external laser radiation at a wavelength of 10.6 μm producing FEL output radiation at a wavelength of 5.3 μm, with an intensity 2×10^7 times larger than spontaneous radiation.

The TESLA Test Facility (TTF) SASE FEL at DESY [34], using the superconducting linac of, up to an energy of 310 MeV, and a 15-m long undulator. The group has reached saturation at a wavelength of 98 nm (see **Figure 4.3**).

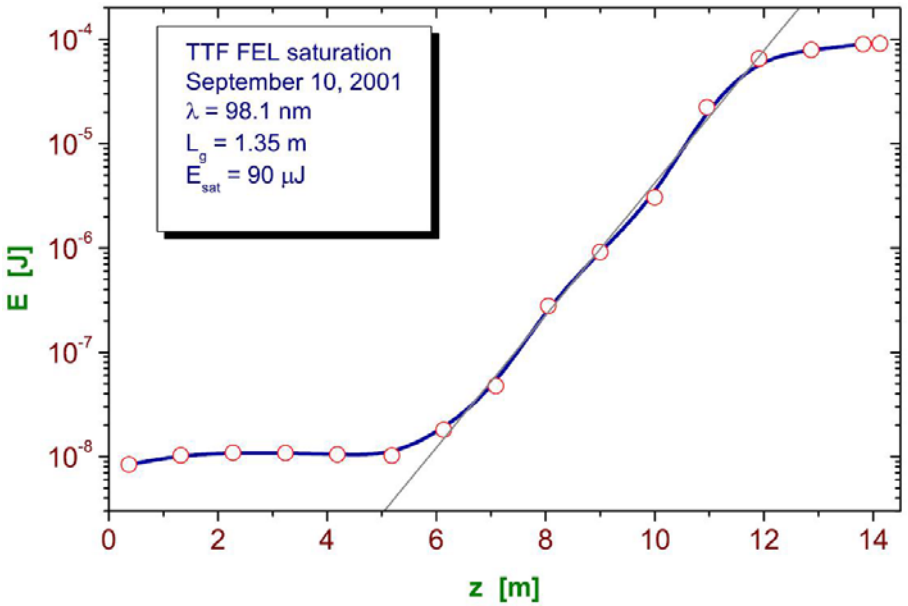

Figure 4.3 The TTF SASE-FEL achieves saturation at a wavelength of 98.1 nm on September 10, 2001.

The LEUTL SASE FEL experiment at the APS [33, 35] using the APS injector linac with an energy range of 220–444 MeV, and a 21.6-m long undulator, has reached saturaton at 530 nm, 385 nm and 130 nm. **Figure 4.4**. shows the saturation at 530 nm (A) and 385 nm (C) as well as output power reduction through the intentional reduction of peak current (B). The solid lines in the figure are simulations using the experimentally measured beam properties. The agreement is very good. The same good agreement was achieved in an absolute comparison of the measured data using measured beam properties to the simulated absolute energy results.

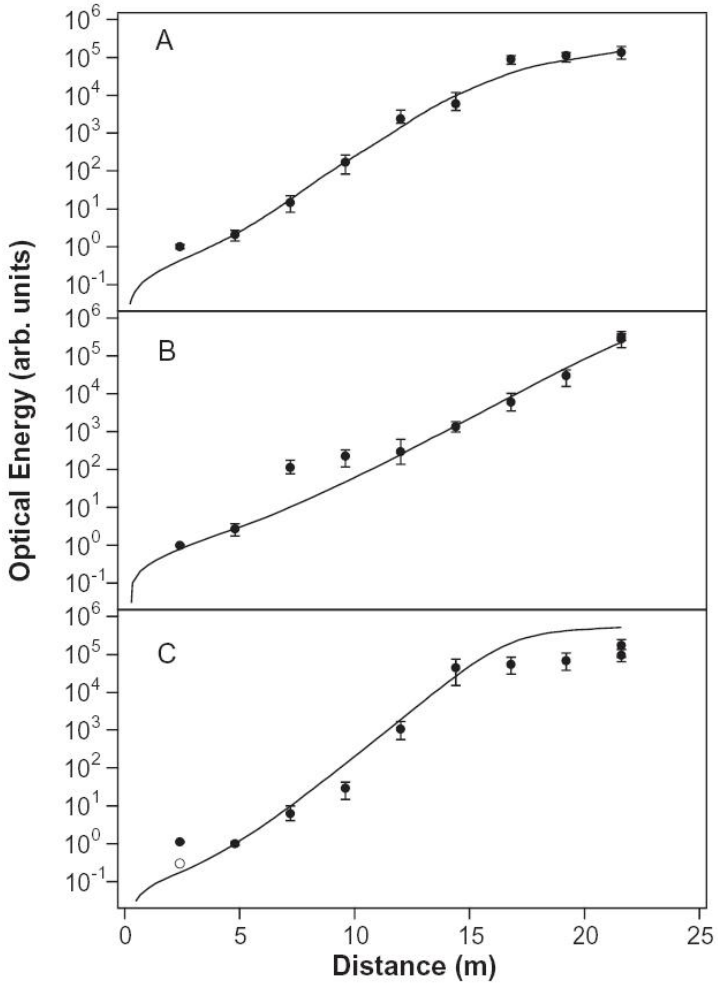

Figure 4.4 Exponential growth and saturation at 530 nm (case A) and 358 nm (case C), in the LEUTL experiment. Case B shows the reduction in gain obtained by reducing the beam current [35].

The VISA experiment, a BNL-LLNL-SLAC-UCLA collaboration, has obtained a gain of about 2×10^8 and reached saturation at a radiation wavelength of 840 nm in 3.6-3.8 m using a 4-m long undulator with distributed strong focusing quadrupoles [36]. The properties of SASE radiation, as a function of distance through the undulator magnet have been measured and analyzed. For the first time, observation and analysis of the statistical intensity fluctuations of SASE radiation at saturation was studied, and compared to the data obtained during exponential growth. These results are compared to the start-to-end numerical model of the experiment, which follows the electron beam dynamics from photocathode emission, through acceleration, transport and the undulator. This combination of experimental results and start-to-end simulations resulted in a comprehensive description of the underlying beam dynamics and FEL process. Additional results based on VISA at saturation include measurements of FEL harmonic radiation and electron beam microbunching. The measured energy of the radiation as function of position along the undulator and the prediction from the numerical model are shown in **Figure 4.5**.

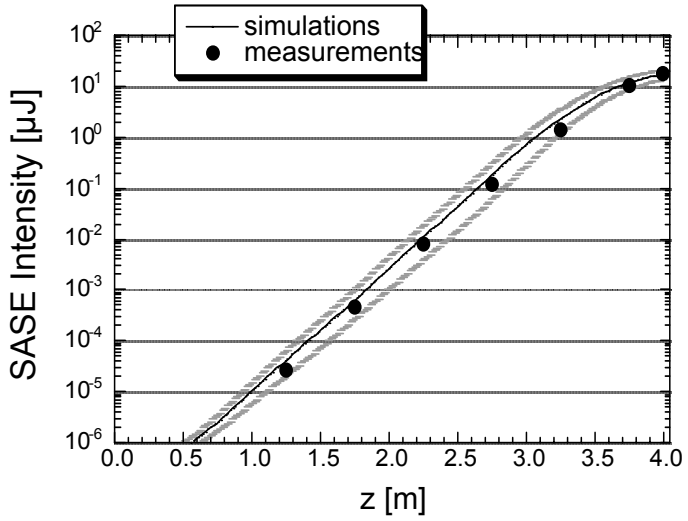

Figure 4.5 Exponential growth and saturation in the VISA experiment at 840 nm, in a 4-m long undulator [36]. The outer curves are the predictions for the 1-sigma limits of the intensity fluctuations.

Similar experimental programs on SASE-FELs are being prepared at Spring8 in Japan, at BESSY-II in Berlin, in China and at other laboratories.

4.4 LCLS: An X-Ray SASE-FEL

The first proposal for a SASE-FEL using the SLAC linac was made in 1992 [21]. The initial design was developed by a study group until 1996 after which a design group prepared the LCLS Design Study Report [23] that was published in 1998.

A short summary of the main LCLS parameters is given in **Table 4.1**. A full list can be found in **Appendix A**. The components of the LCLS and its operational principals are described in full detail in this CDR.

The LCLS will generate coherent radiation at a fundamental wavelength between 15 Å and 1.5 Å. A strong third harmonic component is also produced as discussed above. The LCLS undulator also generates incoherent radiation, which, at the highest electron energy of 14.3 GeV, has a spectrum extending to about 500 keV and a peak power density of 10^{13} W/cm^2, on-axis. The peak coherent power density of the first harmonic is about 2×10^{14} W/cm^2, and the peak electric field is about 4×10^{10} V/m.

The FEL saturation length, the saturation power, and the alignment tolerances depend significantly on the electron beam parameters, and the effect of wakefields in the undulator vacuum pipe, as is discussed in detail in the next sections. Assuming that the electron beam has the parameters given in **Table 4.1**, in particular a 1.2-μm-rad normalized RMS emittance, the SASE amplification process can be simulated.

The simulations are done using the 3D time-dependent code GENESIS 1.3, which includes the effect of quantum fluctuation and wakefields [49]. As can be seen in the next sections, wakefields and quantum fluctuation from the incoherent spontaneous radiation have an effect on the amplification process of a SASE FEL. The GENESIS 1.3 code has been successfully benchmarked with various other FEL codes in the steady-state regime [50], and recently with GINGER for time-dependent simulation. In addition, the simulation of the UCLA/LANL/-RRCKI/SLAC experiment [30] shows good agreement with the experimental data [51].

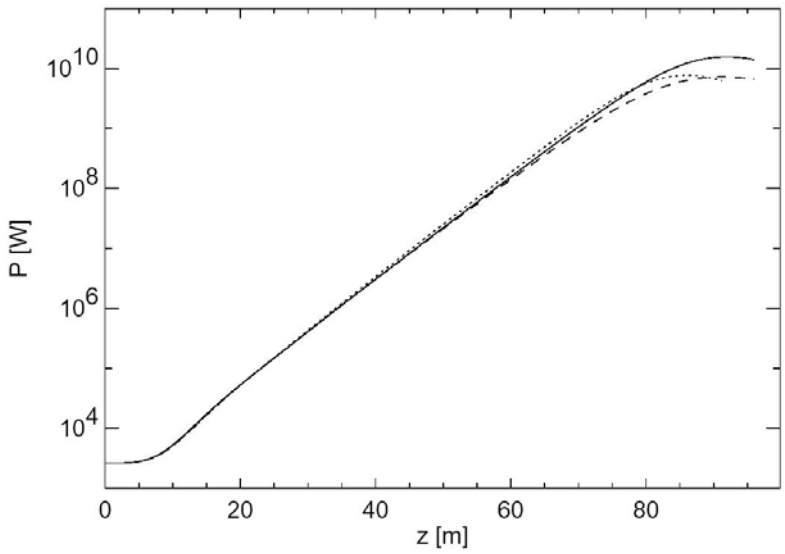

Figure 4.6 Power vs. undulator length for the LCLS case – normalized emittance 1.2 μm rad, peak current 3.4 kA. Solid curve: no wakefields; dotted curve: long roughness bump case; dashed curve: short roughness bump case. The saturation length is about 90 m, and the saturation power levels for the three cases are: 15 GW, 8 GW and 7 GW.

In **Figure 4.6,** power as a function of undulator length is plotted and shows a power gain length of 4.8 m and a saturation length of about 92 m as predicted by GENESIS. The solid curve represents the case where there are no undulator errors, misalignments, and no undulator wakefields. The effect of wakefields is given by the dashed and dotted curves and will be

discussed in the next sections. The effects of errors and misalignments will be discussed in other chapters.

Table 4.1 LCLS electron beam, undulator, and FEL parameters. The electron beam parameters are valid at the undulator entrance.

LCLS Eletron Beam Parameters @1.5 Å	**Value**	**Unit**
Electron energy	14.35	GeV
Peak current	3.4	kA
Normalized RMS slice emittance	1.2	um rad
RMS slice energy spread	1×10^{-4}	
RMS bunch length	77	fs
LCLS undulator parameters		
Undulator period	3	cm
Saturation length (including breaks)	92	m
Peak undulator field	1.32	T
Undulator parameter, K	3.711	
Undulator gap	6	mm
LCLS FEL parameters		
Radiation wavelength	0.15	Å
FEL parameter, ρ	5×10^{-4}	
Power gain length	4.8	m
Effective FEL parameter, ρ_{eff}	2.93×10^{-4}	
Pulses repetition rate	120	Hz
Peak coherent power	8	GW
Peak brightness	0.8×10^{33}	*
Average brightness	4×10^{22}	*
Cooperation length	25	nm
Intrinsic RMS intensity fluctuation	6	%
Number of spikes	270	
RMS line-width	12×10^{-4}	
Total synchrotron radiation energy loss	1.8×10^{-3}	
RMS Energy spread due to synchrotron radiation emission	2×10^{-4}	

* photon/(s mm^2 mrad^2 0.1% BW)

Since a SASE FEL starts from a random noise signal, SASE simulations require many runs with different values for the initial electron positions to reproduce the intensity distribution and obtain mean values for intensity and bunching factor. However, if only mean values are of interest, the amount of CPU time can be significantly reduced by approximating the SASE FEL with an FEL amplifier. The input power level of this equivalent amplifier has been estimated in [38], and this estimate has been used in the simulations. The predicted angular and spectral

distributions of the radiation at the undulator exit are shown in **Figure 4.7** and **Figure 4.8**, for the same case.

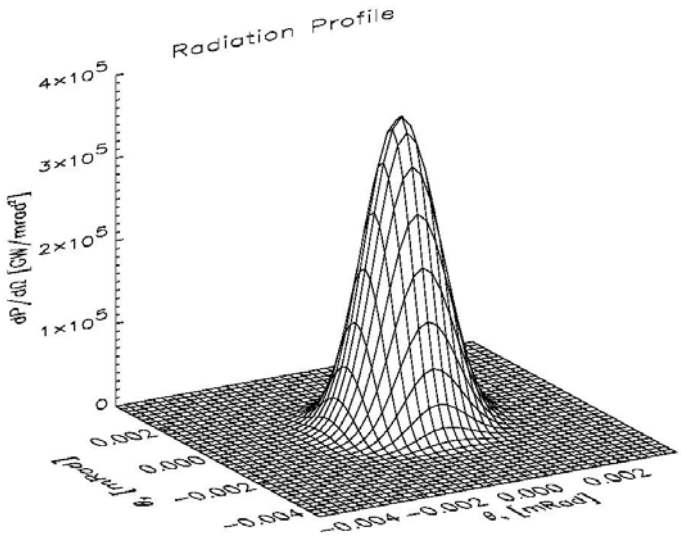

Figure 4.7 Angular distribution of the radiation at the undulator exit, showing a single Gaussian mode, with an rms aperture of about 2 μrad.

Filtering and focusing the radiation and transporting it to the experimental areas is a challenge. A normal incidence mirror at 100 m would see an energy flux density of about 1 J/cm^2, about 1 eV/atom. The large power density of the LCLS x-ray pulses will push the optical elements and instrumentation into a new strong field regime, but also offers new opportunities for scientific research. The development of x-ray optics to handle these large power densities is described in **Chapter 9** of this CDR.

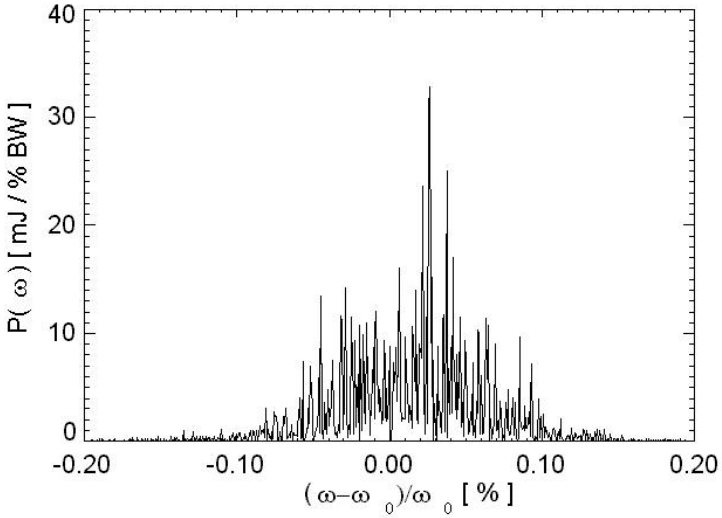

Figure 4.8 Spectral power distribution at undulator exit.

4.5 Effects of Spontaneous Radiation

The emission of spontaneous radiation by electrons in the undulator decreases the average electron energy by W_{eR}, and increases the relative energy spread to $\sigma_{\gamma R}$ [52]. Both effects can reduce FEL gain if the conditions $W_{eR}/E_{beam}<\rho_{eff}$ and $\sigma_{\gamma R}<<\rho_{eff}$ are not satisfied. The two quantities W_{eR} and $\sigma_{\gamma R}$ have been evaluated for the LCLS case and the results are $W_{eR}/E_{beam} \approx 1.8\times10^{-3}$ and $\sigma_{\gamma R} \approx 1.5\times10^{-4}$. When compared to the effective FEL bandwidth, $\rho_{eff} \approx 5\times10^{-4}$, both effects have to be considered. The average energy loss will be different for different electron beam energies but it can be compensated for by micro-tapering the undulator. A large FEL parameter reduces the effect of the energy spread.

4.6 Undulator Wakefields

4.6.1 Wakefield Theory

There are three major sources of wakefields within the undulator vacuum chamber, i.e., resistive wall, geometric, and surface roughness wakefields, which are described in detail in **Chapter 8**. The rest of this section summarizes the basics of undulator chamber wakefields to support the simulation results shown in the next section.

For an x-ray FEL, with a large-peak-current electron beam and a long undulator, the wakefields in the undulator vacuum pipe can have an important effect on the lasing process, reducing the output power and changing the temporal structure of the x-ray pulse. The effect of wakefields becomes noticeable as gain reduction if the condition that the variation in energy be small compared to the gain bandwidth, i.e., $(\Delta E/E)_{wake} < \rho_{eff}$, is satisfied. In the LCLS case, this gives the condition $W_z < 30\ kV/m$ for the longitudinal wakefield amplitude W_z. For every slice in the bunch, for which this condition is fulfilled will be somewhat affected by wakefields. Once the condition is fulfilled the effect growths with the wake-function amplitude.

In ultra relativistic approximation, the resistive longitudinal wakefield [53] from a single electron is

$$W_z(s) = -\frac{4cZ_0}{\pi a^2}\left(\frac{1}{3}e^{-s/s_0}\cos\frac{\sqrt{3}s}{s_0} - \frac{\sqrt{2}}{\pi}\int_0^\infty \frac{x^2 e^{-x^2 s/s_0}}{x^6+8}dx\right), \qquad \textbf{(4.30)}$$

for $s > 0$ and $W_z(s)=0$ for $s < 0$, where s measures the longitudinal position of the test particle with respect to the particle generating the field, Z_0 is the vacuum impedance, $s_0 = (2a^2/Z_0\sigma)^{1/3}$, σ is the conductivity of the material, and a is the pipe radius. For a copper–plated vacuum chamber with a radius of 2.5 mm s_0=8.3 μm and thus comparable with the LCLS rms bunch length of 23 μm.

Geometric wakefields arise if the aperture of the vacuum chamber varies along the undulator. Contributions of bellows, vacuum pump ports, and flanges result in wakefields, which are

typically much smaller than the ones generated by the wall resistance. Thus, they are neglected in the following discussion on the effects of wakefields on the FEL performance.

The first model of surface roughness wakefields [54], which describes the surface as a distribution of bumps covering a smooth surface, results in a severe tolerance on the level of roughness. Based on measurements with an Atomic Force Microscope [55] typical surfaces [56, 57] resemble a smooth surface where the peak-to-valley height, h, is much smaller than the spacing, p, between crests. For a possible prototype of the LCLS undulator vacuum chamber, the RMS height might be h=100 nm while p may exceed tens or even hundreds of microns. A refined model [58], using the small-angle approximation, yields a much more relaxed tolerance on the acceptable roughness.

Both models rely on the condition that the bunch length is much larger than the size of the bumps, which is violated for the short LCLS bunches. Another model [59], valid for the LCLS case and based on a sinusoidal corrugation of the surface with an amplitude h and a wavenumber $k = 2\pi/p$ with $hk<<1$, yields the single-particle wakefield

$$W_z(s) = \frac{cZ_0e^2}{2\sqrt{\pi}}\frac{h^2k^{3/2}}{a}\frac{\partial}{\partial s}\frac{1}{\sqrt{s}}\left[\cos\left(\frac{ks}{2}\right)+\sin\left(\frac{ks}{2}\right)\right]. \qquad \textbf{(4.31)}$$

Comparison shows that the two previous models overestimate the amplitude of wakefields when applied to short bunches.

A. Novokhatski and A. Mosnier pointed out [60] that a periodic, rectangular corrugation also allows synchronous modes (slowed down waveguide modes, which couple to the electron beam.) The wake potential is

$$W_z(s) = -2\kappa\cos(k_0 s) \qquad \textbf{(4.32)}$$

where $\kappa = cZ_0e^2/2\pi a^2$ is the loss factor, $k_0 = \sqrt{2p/hag}$ is the wave number, p is the period, h is the height, and g is the length of the corrugation [61]. Similar results are obtained for a sinusoidal corrugation with an amplitude, h, and a period, $p = 2\pi/k$. If the aspect ratio between height and length of the corrugation becomes small, correction factors have to be applied to the loss factor and the wave number [61, 62], which scale in the limit $h \Rightarrow 0$ as $k_0 = 0$ and $Z = cZ_oe^2/16\pi a^2r^4$ with $r = h\sqrt{ak^3}/2$. For the LCLS with a beam pipe radius of a=2.5 mm, a corrugation amplitude of h=100 nm and a corrugation period, p=100 μm, the correction factor reduces the estimated loss factor, κ, by 10^5, which eliminates any impact on the FEL performance by the synchronous mode.

4.6.2 Wakefield Effects on the LCLS

For the discussion of the impact of wakefields on LCLS performance, the resistive wall wakefields, **Eq. (4.30)**, the roughness wakefields, **Eq. (4.31)**, and the synchronous mode for a sinusoidal corrugation of the vacuum pipe, **Eq. (4.32),** are used. Two cases of roughness wakefields are considered p/h = 50 and 500, both with h = 100 nm. The resulting wake potentials are shown in **Figure 4.9**. The amplitudes of the roughness wakes drop by more than two orders of magnitude towards the longer periodicity and become negligible compared to the resistive wall

wakefield. Atomic Force Microscope measurements [63] of surface roughness gives results in agreement with the second case, $p/\delta = 500$

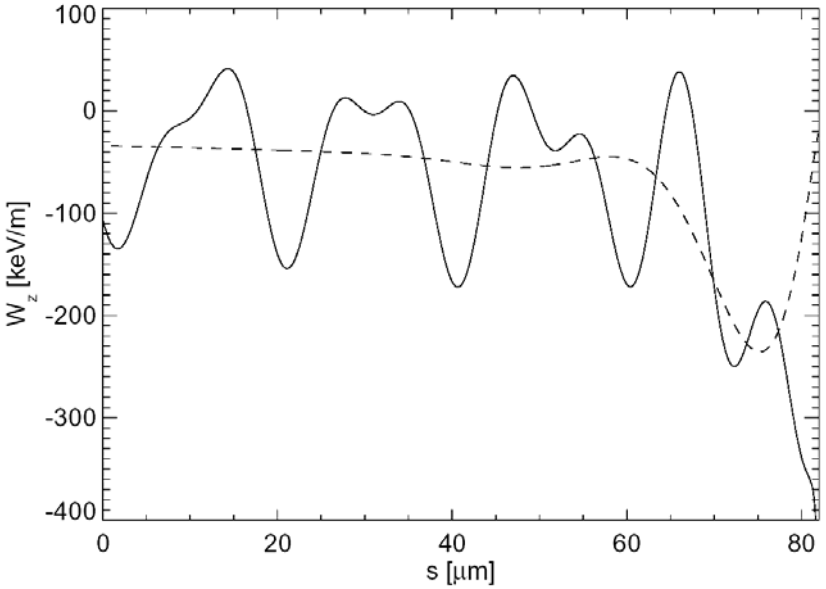

Figure 4.9 LCLS undulator wake potential including the resistive and roughness wakefields. The roughness wakefields include both the inductive model Eq. **(4.31)** and the synchronous mode Eq. **(4.32)**, assuming a 1 nC electron bunch, a bump height of 100 nm, and a bump length of 5 μm (solid line) or 50 μm (dashed line). The resistive wall wakefield dominates the dashed curve. The head of the bunch is at the right hand side of the graph.

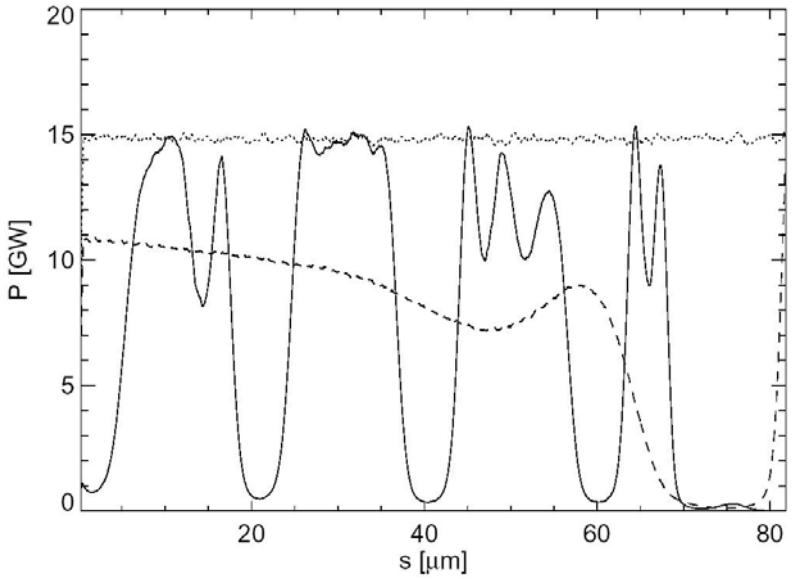

Figure 4.10 Effect of wakefields on the temporal radiation power profile at the undulator exit: Dotted line: no wakefields; dashed line: "long bump case"; solid line: short "bump case". The head of the bunch is at the right hand side of the graph. The simulation includes micro-tapering to offset the energy loss from spontaneous radiation.

The effect of wakefields on the LCLS reference case, evaluated with the simplified model just discussed, is shown in **Figure 4.6**. As one can see from this figure, in the absence of wakefields the peak power is 18 GW. This is reduced to 10 GW for the case of "long bumps", and to 6 GW for the case of "short bumps". The mechanism for this loss of output power is shown in **Figure 4.10**: only the electrons with a small energy loss from wakefields radiate within the gain bandwidth and contribute to the output intensity. The energy loss is small where the total wake potential is close to zero. As a result multiple spikes arise in the power profile for the short bump case (**Figure 4.10**), because the wake potential has multiple zero crossings along the bunch (see **Figure 4.9**). It is also interesting to notice that the gain length is not directly changed by the wakefields (see **Figure 4.6**). It is only in the last part of the undulator that the power is reduced with respect to the zero wakefield case.

4.7 Emittance and Charge Control

As described in the previous sections, the phase-space density, i.e., the transverse and longitudinal emittances, of the electron beam is of critical importance for an x-ray FEL. One method of controlling these properties is to use the photocathode gun laser intensity, spot size and phase to change the charge and minimize the emittance as a function of charge [64, 65, 66]. The scaling laws for transverse emittance and rms bunch length are:

$$\varepsilon = (aQ^{2/3} + bQ^{4/3} + cQ^{8/3})^{1/2}, \tag{4.33}$$

$$\sigma_L = dQ^{1/3} \tag{4.34}$$

where Q is the charge and the three terms in the equation for emittance represent the thermal, space charge and time dependent radio frequency plus chromatic focusing effects respectively. For charges smaller than about 2 nC only the first two terms are important. The values of the coefficients a, b, c, and d depend on the choice of the working point — RF voltage, shape of the laser pulse, and other parameters — of the injector.

Using the Ferrario working point [67], the values of the coefficients are a=0.076 (μm rad)^2/(nC)$^{2/3}$, b=0.18 (μm rad)^2/(nC)$^{4/3}$, d=4.8×10^{-4} m/(nC)$^{1/3}$. The thermal and space charge terms in the emittance are about equal for Q=0.25 nC. The beam brightness, defined as the current over the product of the horizontal and vertical emittances, scales as

$$B = \frac{1}{a + bQ^{2/3}}\ 2.5\times10^{11}\ \frac{\mathrm{C}^{2/3}}{\mathrm{m\ s}}. \tag{4.35}$$

To explore the operational range, we have chosen 2 cases, 0.25 nC and 1 nC in charge. At 0.25 nC, the brightness is close to the best possible value. The emittance and bunch length values are at 0.25 nC: ε~0.24 μm-rad and σL~0.3 mm, and at 1 nC: ε~0.5 μm-rad, and σL~0.48 mm. Photocathode gun simulations at the Ferrario working point, using the Parmela code and including thermal effects, have been done recently for these two cases. The simulations give an emittance of 0.3 μm rad at 0.25 nC and 0.6 μm-rad at 1 nC. These results will be discussed in more detail in the **Chapter 4** in the section about start-to-end simulations of the full LCLS system.

4.8 Control of X-Ray Pulse Length and Linewidth

An FEL has a rather large bandwidth,

$$\frac{\Delta\lambda}{\lambda} = \frac{\lambda}{2\pi L_c} \tag{4.36}$$

where the cooperation length L_c is given by **Eq. (4.25)**. When starting from noise, i.e., in SASE mode, this large gain bandwidth produces spikes in the radiation output as discussed before. Typically for an x-ray SASE FEL the number of spikes is large, about 250 in the LCLS case, hence the pulse length is about 250 times longer than the spike-separation, and the linewidth is about 250 times larger than the Fourier transform limited value for the total bunch length.

Given these physical properties of an FEL, it is in principle possible to reduce the bunch length to that of a single spike, about 1 fs, with a corresponding line width given by **Eq. (4.36)** of the order of 5×10^{-4}. At the other end, it is also possible to eliminate the spikes and produce a single pulse with a length of the order of the bunch length and a line-width of about 2×10^{-6}. Adding the capability of producing x-ray pulses with these characteristics would greatly add to the LCLS usefulness. For this reason both options have actively been explored. The present state of this work can be found in [68] and [69]. Some of the elements of this work are summarized here.

4.8.1 Pulse Length Control

One option to reduce the LCLS pulse length is to reduce the electron bunch pulse length by operating the LCLS compression system in a different configuration. The LCLS has two compression stages. In the reference design, these compressors are used to reduce the electron pulse length from about 10 ps at the electron gun exit to 230 fs at the linac exit. Reference [68] contains a discussion of the possibility of using the two compressors to reduce the electron pulse length to a smaller value. Reducing the pulse length in the compressor to about 10 fs produces very large coherent synchrotron radiation effects. To mitigate these effects, the electron bunch charge has to be reduced to 0.2 nC. Even with the reduced charge the evaluation of the effect of Coherent Synchrotron Radiation (CSR) is open to questions. The current distribution in the bunch is non-uniform, and the energy spread at the linac exit is large, about 0.07%, which is large compared to the LCLS FEL parameter. Such a large energy spread can increase the gain length, and the SASE process for this beam needs to be studied in more detail.

The other method to produce a short bunch is to introduce an energy chirping in the electron bunch [70], thus producing a chirped x-ray pulse and then use optical systems to slice or compress the radiation pulse. To avoid an increase of FEL gain length, the energy chirping of the electrons must be such that the central frequency variation per spike is a fraction of the spike line-width. One of the cases studied in [68] shows that it might be possible to obtain a total electron energy chirping of 2%, corresponding to a total line width of the radiation of 4% and a relative frequency change per spike of 8×10^{-5}, about 1/6 of the spike width.

A chirped x-ray radiation pulse can be sent through a dispersive optical system, followed by another optical system, which selects one "slice" of the pulse. Systems based on Fresnel zone optics or multilayers have been proposed to slice the x-ray pulse. Limitations in the optical systems, differences in optical path lengths — which become important for femtosecond-long pulses — and diffraction effects, limit the obtainable pulse length to the range of 10 fs or larger. A pulse length of about 10 fs corresponds to a selection of about 10 slices out of the 250 of the incoming pulse. The intensity is thus reduced to 4% of the total intensity, and the intensity fluctuations become as large as 30%.

A proposed alternative is to use a double reflecting grating system [71], or a reflecting grating-mirror array system to compress the pulse. Again temporal and diffraction limitation would limit the pulse length to 10 fs or longer. The double grating system has the disadvantage of requiring a longitudinal separation between the two gratings of about 100 m, and of low transmission efficiency. The reflecting grating-mirror array system would eliminate these problems and could produce radiation intensity comparable with the input intensity, and with the same level of intensity fluctuation of the standard LCLS case, about 7%.

A more recent proposal is to use a chirped electron beam, propagating through a first undulator followed by a monochromator, providing a short pulse seed signal for a second undulator [72]. The system can produce 10 fs to 20 fs long pulses, with the same peak power as the LCLS.

The developments of the schemes to reduce the pulse length will require in-depth experimental studies of the electron beam acceleration and compression, of the production and transport before and through the undulator of a beam with a large energy spread, and of the slicing and/or compressing optical systems.

4.8.2 Linewidth Control

Two methods have been studied to reduce the linewidth of a SASE x-ray FEL. One is to follow the High Gain Harmonic Generation (HGHG) scheme with the fresh bunch technique [73, 74]. The other method, the Two-Stage FEL [75], consists of two undulators with an x-ray monochromator located between them. The first undulator operates in the linear high gain regime starting from shot noise in the electron beam. After the first undulator, the output radiation passes through the x-ray monochromator, which reduces the linewidth to the desired value, smaller than the FEL bandwidth. After this monochromator, the intensity fluctuations are 100%. The monochromatization of the radiation is performed at a relatively low level of radiation power, which will reduce damage to the conventional monochromator x-ray optical elements. At the entrance of the second undulator, the monochromatic x-ray beam is then combined with an electron beam and amplified up to the saturation level. The radiation power at the entrance of the second undulator is dominant over the shot noise power, so that the input signal bandwidth is small with respect to the FEL amplifier bandwidth.

The realization of this two-stage FEL scheme for the LCLS requires two undulators 55 and 60 m in length. The output power at the end of the first undulator is 100 MW (which is about 100

times less than the saturation power) with the spectral bandwidth is 5×10^{-4}. Here, an electron beam with an emittance of 1.1 μm-rad and a peak current of 3.4 kA is assumed. The monochromator selects a band, which is wider than the Fourier transform limited bandwidth of approximately 1.5×10^{-6} but smaller than the gain bandwidth. The intensity fluctuation after this monochromator is close to 100%. The total power transmission through the monochromator will be determined by the reflection coefficient of the elements of the monochromator and the ratio of the bandwidth of the monochromator to the bandwidth of the SASE FEL radiation after the first undulator. The reflection coefficient is expected to be in the range of 30%–50%. The monochromator can be considered a linear filter, and therefore, the power distribution after the monochromator will remain a negative exponential distribution. The mean value of the radiation power after the monochromator will be about 100 kW. This is the input radiation power at the entrance of the second undulator and is much greater than the shot noise power. After the monochromator, the radiation pulse can be combined at the entrance of the second undulator with either a new electron bunch or the original electron bunch passed through a bypass (which will remove the electron micro bunching produced in the first undulator). With a mean input radiation power of 100 kW, the second stage would consist of an undulator about 60 m in length. This will allow the FEL process to reach saturation and reduce the intensity fluctuations at the output of the second undulator to less than 10%. In the reference LCLS case the intensity fluctuation is 6%, as shown in **Table 4.1**. The total undulator length needed or this scheme is about 115 m, to which the space needed for the monochromator must be added.

The Two-Stage FEL scheme is compatible with the baseline design of the LCLS presented in this CDR. Its implementation requires the movement of central undulator segments to the beginning of the undulator line, where extra space has been reserved. The total available space for installing the device is about 156 m.

4.9 References

1 H. Motz, *J. Appl. Phys.*, **22**, 527 (1951); H. Motz, W. Thon and R. N. Whitehurst, *J. Appl. Phys.* **24**, 826 (1953); H. Motz and M. Nakamura, *Ann. Phys.* **7**, 84 (1959).

2 R.M. Philips, *IRE Trans. Electron Devices*, **7**, 231 (1960).

3 R.V. Palmer, *J. Appl. Phys.*, **43**, 3014 (1972).

4 K.W. Robinson, *Nucl. Instr. and Meth*, **A239**, 111 (1985).

5 P. Csonka, *Part. Acc.* **8**, 225 (1978).

6 J.M.J. Madey, *J. Appl. Phys.*, **42**, 1906(1971).

7 L.R. Elias, W.M. Fairbank, J.M.J. Madey, H.A. Schwettman and T.I. Smith, *Phys. Rev. Lett.*, **36**, 717 (1976).

8 D.A.G. Deacon, L.R. Elias, J.M.J. Madey, G. J. Ramian, H.A. Schwettman and T.I. Smith, *Phys. Rev. Lett.*, **38**, 892 (1977).

9 N.M. Kroll, Phys. Quantum Electron. 5, 115(1978); P. Sprangle and R.A. Smith, NRL Memo-Report 4033 (1979); A. M. Kondratenko and E.L. Saldin, Dokl. Aka. NAUK SSSR, 249,843 (1979); D. B. McDermott and T. C. Marshall, *Phys. Quantum Electron*. **7**, 509 (1980); A. Gover and P. Sprangle, *IEEE J. Quantum Electron*. **QE-17**, 1196 (1981); G. Dattoli et al., *IEEE J. Quantum Electron*. **QE-17**, 1371 (1981); R. Bonifacio, C. Pellegrini, and L. Narducci, *Opt. Commun.*, **50**, 373 (1984); J.B. Murphy, C. Pellegrini and R. Bonifacio, *Opt. Comm.* **53**, 197 (1985); J. Gea-Banacloche, G.T. Moore and M. Scully, *SPIE* **453**, 393 (1984); P. Sprangle, C.M. Tang and C.W. Roberson, *Nucl .Instr. and Meth*, **A239**, 1 (1985); E. Jerby and A. Gover, *IEEE J. Quantum Electron.* **QE-21**, 1041 (1985); R. Bonifacio, F Casagrande and C. Pellegrini, *Opt. Comm.* **61**, 55 (1987).

10 R. Bonifacio, C. Pellegrini, and L. Narducci, *Opt. Commun.*, **50**, 373 (1984).

11 K.-J. Kim, *Nucl. Instr. and Meth*, A250, 396(1986); J.-M. Wang and L.-H. Yu, *Nucl Instr. and Meth*, **A250**, 484 (1986).

12 G.T. Moore, *Nucl.Instr. and Meth*, **A239**, 19 (1985); E. T. Scharlemann, A. M. Sessler, and J. S. Wurtele, *Phys. Rev. Lett.* **54**, 1925 (1985); M. Xie and D.A.G. Deacon, *Nucl. Instr. and Meth*, **A250**, 426 (1986); K.-J. Kim, *Phys. Rev. Lett.* **57**, 1871 (1986); L.-H. Yu, S. Krinsky and R. Gluckstern, *Phys. Rev. Lett.* **64**, 3011 (1990); Z. Huang and K.-J. Kim, *Nucl. Instr. and Meth*, **A475**, 59 (2001).

13 S. Krinsky and L.-H. Yu, *Phys. Rev.* **A35**, 3406 (1987).

14 M. Xie, *Nucl. Instr. and Meth*, **A445**, 59 (2000); M. Xie, *Nucl.Instr. and Meth*, **A445**, 67 (2000); M. Xie, in Proc. Intern.FEL-2000 Conf., Duke University (2000); Z. Huang and K.-J. Kim, *Phys. Rev.* **E62**, 7295 (2000).

15 A.M. Kondratenko and E. L. Saldin, Part. Acc. 10, 207 (1980); Ya. S. Derbenev, A.M. Kondratenko, and E.L. Saldin, *Nucl. Instr. and Meth*, **A193**, 415 (1982).

16 J.B. Murphy and C. Pellegrini, *Nucl. Instr. and Meth*, **A237**, 159 (1985); J. B. Murphy and C. Pellegrini, J. Opt. Soc. Am. B2, 259 (1985); K.-J. Kim et al., *Nucl. Instr. and Meth*, **A239**, 54 (1985).

17 C. Pellegrini, "Progress Toward a Soft X-ray FEL", *Nucl. Instr. and Meth*, **A272**, 364 (1988).

18 J.S. Fraser, R.L. Sheffield, and E.R. Gray, "A new high brightness electron injector for free-electron lasers driven by RF linacs," *Nucl.Instr and Meth*, **A250**, pp. 71-76, 1986.

19 B. E. Carlsten *Nucl.Instr and Meth*, **A285**, 313-319 (1989); X. Qiu, K. Batchelor, I. Ben-Zvi, and X-J. Wang, "Demonstration of Emittance Compensation through the Measurement of Slice Emittance of a 10 ps Electron Pulse", *Phys. Rev. Lett.* **76**, 3723-3726 (1996).

20 K. Bane, "Wakefield Effects in a Linear Collider", *AIP Conf. Proc*., vol. **153**, p. 971 (1987); J. Seeman et al, "Summary of Emittance Control in the SLC Linac", *US Particle Accelerator Conference, IEEE Conf. Proc. 91CH3038-7*, p. 2064 (1991); J. Seeman et al, "Multibunch Energy and Spectrum Control in the SLC High Energy Linac", *US Particle Accelerator Conference, IEEE Conf. Proc. 91CH3038-7*, p. 3210 (1991); T. Raubenheimer, "The Generation and Acceleration of Low Emittance Flat Beams for Future Linear Colliders", SLAC-Report 387 (1991).

21 C. Pellegrini, "A 4 to 0.1 nm FEL based on the SLAC Linac", in Proc. of the Workshop on IV Generation Light Sources, M.Cornacchia and H. Winick eds., SSRL-SLAC Report 92/02, p. 364 (1992).

22 C. Pellegrini et al., "The SLAC Soft X-ray High Power FEL", *Nucl. Instr. and Meth*, **A341**, 326 (1994); G. Travish et al., "Parametric Study of an X-ray FEL", *Nucl. Instr. and Meth*, **A358**, 60 (1995).

23 LCLS Design Study Report, Report SLAC-R-521, (1998).

24 J. Rossbach et al., *Nucl. Instr. and Meth*, **A375**, 269 (1996).

25 T. Orzechowski et al., *Phys. Rev. Lett.* **54**, 889 (1985); D. Kirkpatrick, *Nucl. Instr. and Meth*, **A285**, 43 (1989); J. Gardelle, J. Labrouch and J.L. Rullier, *Phys. Rev. Lett.* **76**, 4532 (1996).

26 R. Prazeres et al., *Phys. Rev. Lett.* **78**, 2124 (1997).

27 M.Hogan et al., "Measurements of High Gain and Intensity Fluctuations in a SASE free-electron laser", *Phys. Rev. Lett.* **80**, 289 (1998).

28 M. Babzien et al., "Observation of self-amplified spontaneous emission in the near-infrared and visible wavelengths", *Phys. Rev.* **E 57**, 6093-6100 (1998).

29 D. C. Nguyen et al., "Self Amplified Spontaneous Emission Driven by a High-Brightness Electron Beam", *Phys. Rev. Lett.* , **81**, 810-13 (1998).

30 M. Hogan et al., "Measurements of Gain larger than 10^5 in a 12 μm SASE-FEL", *Phys. Rev. Lett.* **81**, 4867-4870 (1998).

31 L.-H. Yu et al, " First Lasing of a High-Gain Harmonic Generation Free-electron Laser Experiment", *Nucl. Instr. and Meth*, **A445**, 301 (1999), and *Proc. Intern.FEL-2000 Conf., Duke University* (2000).

32 A. Tremaine et al., "Initial Gain Measurements of a 800 nm SASE-FEL, VISA", in *Proc Intern.FEL-2000 Conf., Duke University* (2000);

33 S. V. Milton et al., "Observation of Self-Amplified Spontaneous Emission and Exponential Growth at 530nm," *Phys. Rev. Lett.*, **85**, 988-991 (2000), and *Proc. Intern.FEL-2000 Conf., Duke University* (2000).

34 J. Rossbach et al., "Observation of Self amplified Spontaneous Emission in the wavelength range from 80 nm to 180 nm at the TESLA test facility FEL at DESY", in *Proc. Intern.FEL-2000 Conf., Duke University* (2000); J. Andruszkow et al., *Phys. Rev. Lett.* **85**, 3825-3829 (2000).

35 S. Milton and al. Science E*xpress,* May 17, (2001).

36 A. Tremaine et al., "Saturation Measurements of an 800 nm SASE FEL," in *Proc. of the 23th International Free Electron Laser Conference Darmstadt, Germany,* (2001).

37 J. B. Murphy and C. Pellegrini, "Introduction to the Physics of Free-Electron Lasers," in Laser Handbook, Vol. 6, W.B. Colson, C. Pellegrini, and A. Renieri eds., North Holland, (1990); R. Bonifacio et al., *La Rivista del Nuovo Cimento*, Vol. 13, N. 9, (1990).

38 R. Bonifacio, et al, "Spectrum, Temporal Structure, and Fluctuations in a High Gain Free-electron Laser Starting from Noise," *Phys. Rev. Lett.,* **73**, 70 (1994).

39 E.L. Saldin, E.A. Schneidmiller, and M.V. Yurkov, "Statistical properties of Radiation from VUV and X-ray Free Electron Laser", DESY rep. TESLA-free-electron laser 97-02, (1997).

40 R. Bonifacio, L. De Salvo and P. Pierini, *Nucl. Instr.and Meth*, **A293**, 627 (1990); H.P. Freund, S.G. Biedron and S.V. Milton, *IEEE J. Quantum Electron.*, **QE-36**, 275 (2000); *Nucl. Instr.and Meth*, **A445**, 53 (2000); M. Xie, *Nucl. Instr and Meth*, **A475**, 51 (2001).

41 L.H. Yu, *Phys. Rev.* **A44**, 5178 (1991).

42 Z. Huang and K.-J. Kim, *Phys. Rev.* **E 62**, November, 2000; *Nucl. Instr.and Meth*, **A475**, 112 (2001).

43 R. Bonifacio, “On the classical and quantum feature of self amplified spontaneous emission”, in Towards X-ray Free Electron Lasers, R. Bonifacio and W. A. Barletta eds, *AIP Conf. Proc.* **413**, p. 15 (1997).

44 K.-J. Kim, “Temporal and transverse coherence of self amplified spontaneous emission”, in Towards X-ray Free Electron Lasers, R. Bonifacio and W. A. Barletta eds, *AIP Conf. Proc.* **413**, p. 3 (1997).

45 C. Schroeder, C. Pellegrini, and P. Chen, "Quantum Fluctuations in Free-Electron Lasers", incourse of publication in *Proc. Of the 2nd Conf. on Quantum Aspects of Beam* Physics, Capri (2000).

46 M.C. Teich, T. Tanabe, T.C. Marshall and J. Galayda, *Phys. Rev. Lett*. **65**, 3393 (1990).

47 W.M. Fawley, LBNL Report LBNL-49625 (2002).

48 E. L. Saldin, E. A. Schneidmiller, M. V. Yurkov, " Numerical simulation of the UCLA-LANL-RRCKI-SLAC experiment on a high gain SASE FEL", *Nucl. Instr. and Meth*, **A429**, 197-201 (1999).

49 S. Reiche, *Nucl. Instr. and Meth*, **A429**, 243 (1999).

50 S.G. Biedron et al*., Nucl. Instr. and Meth*, **A445** (2000) 110.

51 S. Reiche, DESY-Print, DESY-THESIS-2000-012 (2000)

52 E.L. Saldin et al., *Nucl. Instr. and Meth*, **A381**, 545 (1996).

53 K. Bane, SLAC report AP-87 (1991).

54 C.-K. Ng, *Phys. Rev.* **D42**, 1819 (1990); K. Bane, C.-K. Ng, and A. Chao, "Estimate of the impedance due to wall surface roughness," SLAC-PUB-7514, (1997).

55 G.L. Stupakov et al., "Effects of beam tube roughness on a X-Ray free-electron laser performance," *Phys. Rev. ST* **2**, 60701/1-60701/6 (1999).

56 D.J. Whitehouse, Handbook of Surface Metrology (IOP Publishing, 1994)

57 K.J. Stout, Atlas of Machined Surfaces (Chapman and Hall, 1990).

58 G. V. Stupakov, *Phys. Rev. ST Accel. Beams* **1**, 064401 (1998).

59 G.V. Stupakov, "Surface Roughness Impedance." *AIP Conference Proceedings* **581**, p 141-152, ISBN 0-7354-0022-9, ISSN 0094-243X (2000).

60 A.V. Novokhatskii and A. Mosnier, *Proc. 1997 Particle Accelerator Conf*., 1661-1663 (1997).

61 K.L. Bane and A.V. Novokhatskii, SLAC, Tech. Rep. SLAC-AP-117 (1999).

62 G. V. Stupakov, in T. Roser and S. Y. Zhang, eds., Workshop on Instabilities of High Intensity Hadron Beams in Rings (American Institute of Physics, New York, 1999), no. 496 *in AIP Conference Proceedings*, pp. 341-350.

63 G. Stupakov, R.E. Thomson, D. Walz, and R. Carr, "Effects of Beam Tube Roughness on X-Ray Free Electron Laser Performance," *Phys. Rev. ST Accel. Beams,* **2**(6), 060701/1-60701/6 (1999).

64 J. B. Rosenzweig and E. Colby, in *AIP Conf. Proc*., vol.**335**, p. 724 (1995).

65 J. B. Rosenzweig et al., "Optimal Scaled Photoinjector Designs for FEL Applications", in *Proc. IEEE Part. Acc. Conf*., p. 2045 (1999).

66 J. B. Rosenzweig, private communication.

67 M. Ferrario et al, New Design Study and Related Experimental Program for the LCLS RF Photoinjector**,"** LCLS-TN-00-9 (2000).

68 V. Bharadwaj et al. "Ultrashort Light Pulses in the LCLS", LCLS-TN-00-08, SLAC (2000).

69 "LCLS: the first experiments", Report of the LCLS Scientific Advisory Committee, SLAC (2000).

70 P. Emma, "Chirping the LCLS Electron Beam." LCLS-TN-00-6, (2000).

71 C. Pellegrini, ":High Power femtosecond pulses from an X-ray SASE-FEL", *Nucl. Instr. and Meth*, **A445**, 124-127 (2000).

72 C. Schroeder et al., “Chirped-Beam Two-Stage SASE-FEL for High Power Femtosecond X-ray Pulse Generation”, in *Proc. of the 2001 Particle accelerator Conf., Chicago 200*1, in course of publication.

73 I. Ben-Zvi, K. M. Yang and L.-H. Yu, *Phys. Rev.* **A318**, 726 (1992)

74 L.-H. Yu et al., in *Proc. of the 22nd Intern. FEL Conf.*, Duke University (2000)

75 J. Feldhaus, E. L. Saldin, J. R. Schneider, E. A. Schneidmiller, and M. V. Yurkov, "Possible application of X-ray optical elements for reducing the spectral bandwidth of an X-ray SASE FEL", *Opt. Commun.* **140**, 341-352 (1997); E. L. Saldin, E. A. Schneidmiller, Y. V. Shvyd'ko, and M.V. Yurkov, "X-ray FEL with a meV Bandwidth", in *Proceedings of the 22nd International Free Electron Laser Conference, Durham, 2000* (Elsevier, Amsterdam, in press); E. L. Saldin, E. A. Schneidmiller, and M. V. Yurkov, "Optimization of a seeding option for the VUV free electron laser at DESY", *Nucl. Instr. and Meth*, **A445**, 178-182 (2000).